Femtosecond photoassociation: Coherence and implications for control in bimolecular reactions

Peter Gross and Marcos Dantus
Department of Chemistry, Michigan State University, East Lansing, Michigan 48824-1322

(Received 4 December 1996; accepted 14 February 1997)

A theoretical analysis of the recent femtosecond photoassociation spectroscopy (FPAS) experiment on mercury [U. Marvet and M. Dantus, Chem. Phys. Lett. **245**, 393 (1995)] is presented. It is shown that when a thermal distribution of diatom collision pairs is excited from a free to a bound electronic state on a time scale shorter than molecular vibration, an ensemble of coherent wave packets is produced. The dynamics of these wave packets created by the photoassociation pulse can be observed by firing a second probe pulse at variable time delays, and the depletion of the first excited bound state by the probe pulse is detected via fluorescence of the remaining population. Simulations of the FPAS experiment, using both wave packet propagation techniques and perturbation theory, clearly show the vibrational dynamics of the photoassociated transients. It is also demonstrated how the FPAS technique may be used as a tool for controlling the energy, impact parameter, and orientation in bimolecular reactions. © *1997 American Institute of Physics.* [S0021-9606(97)01819-9]

I. INTRODUCTION

The photoassociation process consists of a free-to-bound optical transition which causes bond formation between colliding reactants and can be considered as the reverse of unimolecular photodissociation.[1–5] Photoassociation has been employed to study the long range molecular states near the dissociation limit of diatomic ground state potentials between optically cooled atoms.[6–9] These studies provide information on the long range form of the internuclear ground state potential. As an alternative to emission spectroscopy, photoassociation spectroscopy has also been used to study the lowest excited state potential of diatomics whose ground electronic states are dissociative as in the case of KrF[10,11] and XeCl,[12] and metal excimers.[13–15]

To date, most photoassociation studies like the ones cited above have been based on frequency resolved spectra. Recently, however, time resolved femtosecond photoassociation spectroscopy (FPAS) has been performed on mercury by Marvet and Dantus.[16] In this experiment, randomly distributed mercury atoms in thermal equilibrium were optically excited from the (nearly) purely repulsive XO_g^+ ground state to the bound $D1_u$ excited state via a 60 fs pump (or bind) pulse of wavelength 312 nm. The prepared wave packet on the $D1_u$ potential was then subsequently probed with a 624 nm pulse of similar duration. Their experiment showed the bond formation to occur within the duration of the femtosecond bind pulse. Rotational coherence was detected by monitoring the rotational anisotropy of the FPAS transients as a function of bind-probe time delay, vibrational coherence of the photoassociated transients was not conclusively observed. In this work we develop a theoretical framework to simulate time resolved photoassociation experiments in order to address the issue of vibrational coherence and to evaluate their potential for control of bimolecular reactions.

Wing absorption and emission spectroscopy have long been recognized as direct probes of the ultrafast dynamics of atomic collisions,[17,18] and those of dissociation ''half collision'' processes.[19] The technique of femtosecond transition state spectroscopy (FTS) in fact utilizes this principle to probe the transition state dynamics of chemical reactions *directly*.[20] Glownia *et al.* have obtained femtosecond time resolved absorption spectra of dissociating thallium iodide[21] and Bi_2 molecules[22] and have shown that the wing absorption extends hundreds of wavenumbers when the atoms are still in close proximity. The aforementioned photoassociation experiments by Marvet and Dantus[16] take advantage of the wing absorption due to the steady state population of collision pairs present in gaseous mixtures to induce bimolecular chemical reactions with a given orientation, alignment, and energy.

Time resolved studies of bimolecular reactions have been mainly carried out starting from van der Waals precursors which maintain a restricted alignment and upon photoinitiation release one of the reactants at a specific initiation time.[23–25] In a different approach, excitation of iodine molecules in the presence of xenon has been used to control the yield of XeI.[26] The FPAS experiments on mercury were achieved with a binding laser that was 7370 cm^{-1} away from resonance of the free fragments,[16] ensuring that only those fragments undergoing a collision are excited. The probe interrogates the photoassociated molecules, thereby revealing the time resolved dynamics following bond formation.

There have been some theoretical studies on the subject of photoassociation with ultrafast pulses. Krause, Shapiro, and Brumer proposed the use of picosecond lasers to coherently control the collinear reaction of monoenergetic $H+H_2$.[27] More recently, transition probabilities to excited bound electronic states from the dissociative ground state of several Rydberg molecules were examined.[28,29] These calculations were performed under the ''frozen nuclei'' approximation,[28] meaning that the internuclear distance between atom pairs was assumed to be fixed over the photoassociation pulse duration. To check this approximation, the authors also performed a full multicurve wave packet calcu-

 0021-9606/97/106(19)/8013/9/$10.00

lation on one of the systems, NeH. However, for this calculation, the initial wave packet was taken to be the ground vibrational eigenstate of the lowest excited bound electronic state of NeH (and therefore was implicitly assumed to be comprised of a coherent superposition of states).

Although formally the total transition probability from a dissociative electronic state to another (bound or dissociative) state should be calculated by performing the incoherent summation over the transition probabilities from all (Boltzmann-weighted) continuum eigenstates,[30,31] the justification for using the initial wave packet state was presumably the assumption that the NeH was a product of dissociation of a van der Waals precursor, as discussed above.

In another study, Jiang and Hutchinson studied the free-bound radiative excitation in the transition state region of the reaction $K+NaCl \rightarrow KCl+Na$.[32] As in the previously mentioned studies,[28,29] the initial state was taken as a coherent superposition of continuum states (i.e., a wave packet). The width of this wave packet which enters the transition state regime on the ground surface was arbitrarily chosen as a Gaussian with a particular width, and no averaging over relative velocities between the collision partners was performed.

More recently, two theoretical papers have been published which deal with time resolved photoassociation.[33,34] In the first of these, photoassociation of ultracold sodium dimers was considered. Due to the sub-milli Kelvin temperature of the system, only a very narrow range of continuum vibrational states was assumed to be populated in the ground electronic state. The second work by Backhaus and Schmidt[34] simulates the same mercury FPAS experiment as this work and confirms the rotational and vibrational coherence taking into account the much broader distribution of continuum states populated at the relatively high temperature of the system (433 K).

In both of these time resolved ultrafast theoretical photoassociation studies it was predicted that vibrational transients of the photoassociated bound complex could be observed with a variable pump (or here bind) probe time delay. Although vibrational transients have been observed previously in femtosecond pump-probe studies, for example those of Zewail and co-workers at Caltech,[35,36] it should be noted that in these systems the initial state was comprised of a finite number of bound eigenstates whose transition was followed by detectable vibrational motion on the (bound or dissociative) excited state surface. In contrast, the initial state in the photoassociation experiments is comprised of a thermal distribution of continuum states, and so the question which arises is whether or not transitions from this continuum of states would ''smear out'' vibrational coherent dynamics in the excited state bound potential of the photoassociated species. In the case of the ultracold sodium atoms, this was not an issue since only a narrow thermal range of continuum states was assumed to be populated,[33] but for the previous study[34] on mercury and this work where large temperatures and a broad distribution of incoherent states are assumed the question of generating a coherent wave packet becomes more relevant.

In this and the previous work on mercury photoassociation,[34] it is demonstrated that indeed a coherent wave packet is formed from an incoherent ensemble in the ground electronic state. Vibrational transients of the photoassociated product are simulated both using wave packet propagation and perturbative techniques. The wavelength of the bind laser determines the degree of localization of the wave packet which is primarily dictated by the Franck–Condon overlap between the free and bound states. Vibrational coherence, however, can only be observed if the wave packet motion is slower than the duration of the laser pulse. This can be achieved for most molecular systems given the recent advances in femtosecond laser technology.

In addition to providing a new tool for the time resolved study of bimolecular chemical reactions, we also demonstrate how the FPAS method can be used to control the energy, orientation, and impact parameter of these processes. We present calculations which show that one may control the impact parameter of the colliding pairs which are photoassociated by varying the laser bind wavelength. Control of the impact parameter will allow for control of the photoassociated product angular momentum especially for reactants with narrow kinetic energy distributions.

This paper is organized as follows. In Sec. II we outline the basic theory behind the simulations of the mercury FPAS experiments. Both nonperturbative (wave packet propagation) and perturbative methods are used to compute the fluorescence from the $D1_u$ state as a function of bind-probe time delay. In Sec. III a discussion of the physical significance of the computed FPAS signal is presented, and we consider the effect of multiple probe depletion states as a possible reason for not observing a clear (sinusoidal) vibrational transient signal in the FPAS experiments. Also discussed here is the approximation of including only zero impact parameter collisions of mercury atoms prior to photoassociation in our calculations. Section IV provides concluding remarks including how FPAS experiments may be relevant to laser-induced control of bimolecular reactions with regard to alignment, energy, and impact parameter.

II. THEORY

The relevant diatom mercury potentials $V_1(R)$, $V_2(R)$, and $V_3(R)$ corresponding to the XO_g^+, $D1_u$, and 1_g states, respectively, are shown in Fig. 1. All three curves are modeled as Morse potentials (see Table I for parameters). The bind and probe pulses are shown schematically on Fig. 1 as well. All mercury atom pairs photoassociated up to the $D1_u$ state by the bind pulse are assumed to fluoresce back down to the ground state if no probe pulse is applied; the probe pulse depletes the $D1_u$ state thereby decreasing the experimentally detectable fluorescence from this state.

As mentioned in Sec. I, two methods are used to simulate the Hg+Hg FPAS experiment. The first to be described is based on standard numerical wave packet propagation techniques in which the effect of the (more intense) probe pulse on the excited state transient is treated nonperturbatively. The initial continuum eigenstates are taken as standard WKB wavefunctions:

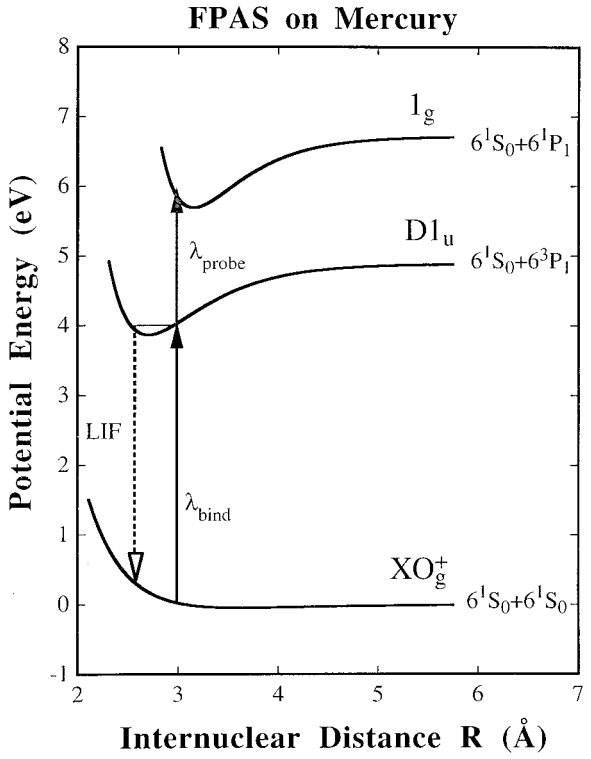

FIG. 1. Relevant potential energy curves in the FPAS experiment on mercury. Also shown schematically are the bind and probe pulse excitation pathways.

$$|\phi_E(R)\rangle = \frac{2N}{\sqrt{k(R)}} \cos\left(\int_{R_C}^{R} dR' k(R') - \frac{\pi}{4} \right); \quad R > R_C, \tag{1a}$$

$$|\phi_E(R)\rangle = \frac{N}{\sqrt{\kappa(R)}} \exp\left[\int_{R_C}^{R} dR' \kappa(R') \right]; \quad R < R_C, \tag{1b}$$

where R_C is the classical turning point on $V_1(R)$ at energy E, i.e., $V_1(R_C)=E$, $k(R')=\sqrt{2m[E-V_1(R')]}/\hbar$, $\kappa(R')=\sqrt{2m(V_1(R')-E)}/\hbar$, m is the reduced mass of the mercury dimer, and N is the normalization constant. The wave packet created on $V_2(R)$ by the bind pulse is computed using first-order perturbation theory:[37,38]

$$|\psi_2(R,\tau)\rangle = -\frac{i}{\hbar} \int_0^{\tau} dt \, \exp[-iH_2(\tau-t)/\hbar] \mu_{21}(R) \epsilon_{\text{bind}}(t) \times \exp(-iEt/\hbar) |\phi_E(R)\rangle, \tag{2}$$

where $H_2 = T + V_2(R)$ is the Born–Oppenheimer Hamiltonian of the $D1_u$ state, $\mu_{21}(R)$ is the electronic transition dipole moment between the XO_g^+ and $D1_u$ states, and E is the energy of the continuum eigenstate $|\phi_E(R)\rangle$. The fast Fourier transform (FFT) split-operator method[39] was used to evaluate the propagator in Eq. (2).

The bind pulse form is taken as a Gaussian:

$$\epsilon_{\text{bind}}(t) = A_{\text{bind}} \exp[-\alpha^2 (t-t_{\text{bind}})^2] \cos(\omega_{\text{bind}} t), \tag{3}$$

where $A_{\text{bind}}=0.001$ a.u. (corresponding to a peak intensity of $\approx 10^{10}$ W/cm^2), $\alpha = 0.000\,671\,7$ a.u. [corresponding to an intensity full width at half maximum (FWHM) of 42 fs], and $\omega_{\text{bind}}=0.1460$ a.u. (corresponding to a bind pulse wavelength of 312 nm). At the end of the bind pulse propagation ($\tau = 2t_{\text{bind}}$), the probe pulse is fired at various time delays. Its form is also Gaussian,

$$\epsilon_{\text{probe}}(t) = A_{\text{probe}} \exp[-\alpha^2 (t-t_{\text{probe}})^2] \cos(\omega_{\text{probe}} t), \tag{4}$$

only here the field is more intense, $A_{\text{probe}} = 10 A_{\text{bind}}$, and the photon energy halved, $\omega_{\text{probe}} = 0.5\omega_{\text{bind}}$. The minimum bind-probe time delay, defined as $t_{\text{probe}} - t_{\text{bind}}$, is $2t_{\text{bind}}$ since the computations are simplified greatly if the bind and probe pulses are assumed not to overlap.

TABLE I. Morse potential parameters for Hg_2 curves.

	ω_e (cm^{-1})	$\omega_e\chi_e$ (cm^{-1})	D_e (cm^{-1})	R_e (Å)	$V(R=\infty)$ (eV)
XO_g^+	19.6[a]	0.26[a]	370[a]	3.63[a]	0
$D1_u$	127[a]	0.50[a]	8100[a]	2.50[a]	4.89[a]
1_g	150[b]	0.213[c]	8260[c]	3.15[c]	6.75[c]

[a]Reference 45.
[b]Reference 46.
[c]Reference 16.

The interaction of the probe pulse on the wave packet which has been excited up to $V_2(R)$, $|\psi_2(R,\tau)\rangle$, is described by the coupled time-dependent Schrodinger equation (TDSE):

$$i\hbar \frac{\partial}{\partial t} \begin{bmatrix} \psi_2(R,t) \\ \psi_3(R,t) \end{bmatrix} = \begin{bmatrix} H_2 & \mu_{23}(R)\epsilon_{\text{probe}}(t) \\ \mu_{32}(R)\epsilon_{\text{probe}}(t) & H_3 \end{bmatrix} \times \begin{bmatrix} \psi_2(R,t) \\ \psi_3(R,t) \end{bmatrix}. \tag{5}$$

To compute the FPAS vibrational transient signal, we recall that without the probe pulse all photoassociated molecules in the $D1_u$ state created by the bind pulse eventually fluoresce back down to the ground state. Thus the probe pulse, which causes a depletion of population in the $D1_u$ state by transferring it to the 1_g state, causes a proportional decrease in the fluorescence which may be expressed as

$$F = \frac{P_2 - P_3}{P_2}, \tag{6}$$

where $P_2 = \langle \psi_2(R,\tau) | \psi_2(R,\tau) \rangle$, i.e., the population on $V_2(R)$ before the probe pulse is applied, and P_3 is the population on $V_3(R)$ after the probe pulse.

If L Boltzmann-weighted continuum states are included in the calculation, then

$$P_2 = \frac{1}{N^2} \sum_{l=1}^{L} \exp(-E_l/k_B T) \langle \psi_2^{(l)}(R,\tau) | \psi_2^{(l)}(R,\tau) \rangle, \tag{7}$$

where $|\psi_2^{(l)}(R,\tau)\rangle$ is computed from Eq. (2) assuming the initial continuum eigenstate $|\phi_{E_l}\rangle$. Likewise, the population on $V_3(R)$ after the probe pulse is

$$P_3=\frac{1}{N^2}\sum_{l=1}^{L}\ \exp(-E_l/k_BT)\langle\psi_3^{(l)}(R,\tau)|\psi_3^{(l)}(R,\tau)\rangle. \quad (8)$$

Note that the excitation process is *coherent* with respect to each continuum state [see Eq. (2)], but the sum over the L initial continuum eigenstates is incoherent because of their thermal distribution [see Eqs. (7) and (8)]. The incoherent superposition of states behaves as a coherent ensemble provided that the time scale of excitation is shorter than the time scale of atomic motion in the excited state. In practice, a similar restriction applies to the observation of coherent wavepacket motion in bound to bound excitation. All states $|\phi_{E_l}\rangle$ were chosen over a range of energy from 0 to 0.33 eV; this range adequately covers the thermally accessible states at the temperature in the experiment ($T=433$ K).

Since the coupled TDSE in Eq. (5) must be solved for many different bind-probe time delays in order to obtain a reasonably resolved signal from which we can elucidate the vibrational dynamics on $V_2(R)$, this quantum-mechanically more rigorous method is computationally expensive. An alternative, approximate but computationally less demanding method which relies totally on time-dependent perturbation theory is described below.

Let $|\phi_E\rangle$ be a continuum eigenstate of $V_1(R)$ as before, and let $|\phi_2^{(m)}\rangle$ and $|\phi_3^{(n)}\rangle$ be the mth and nth bound eigenstates of $V_2(R)$ and $V_3(R)$, respectively. Ignoring the higher continuum vibrational states of $V_2(R)$, the wavefunction at any time t on $V_2(R)$ can simply be expressed as

$$|\psi_2(R,t)\rangle=\sum_m\ a_2^{(m)}(t)|\phi_2^{(m)}\rangle. \quad (9)$$

The population on $V_2(R)$ after the bind pulse at time $t=\tau$ is therefore

$$\begin{aligned}\langle\psi_2(R,\tau)|\psi_2(R,\tau)\rangle&=\sum_m\ |a_2^{(m)}(\tau)|^2=\frac{\pi\mu_{21}^2A_{\rm bind}^2}{4\alpha^2\hbar^2N^2}\sum_m\ \sum_E\ |\langle\phi_2^{(m)}|\phi_E\rangle|^2\\&\quad\times\exp[-(\omega_{mE}-\omega_{\rm bind})^2/4\alpha^2]\\&\quad\times\exp(-E/k_BT),\end{aligned} \quad (10)$$

where the summation m is over all bound states of $V_2(R)$ and $\omega_{mE}=(E_m-E)/\hbar$. Although the energy levels above $E=0$ on the ground state are continuous, in actual computations we perform a summation over discretized energies as shown in Eq. (10). (Convergence with respect to the range of E, i.e., the maximum energy value in the summation over the Boltzmann-weighted continuum states, was checked.) The $\exp(-E/k_BT)$ factor represents the Boltzmann weighting of the initial continuum states, and the $\exp[-(\omega_{mE}-\omega_{\rm bind})^2/4\alpha^2]$ term results from integrating the product of the binding pulse and $\exp(-i\omega_{mE}t)$ over time in accordance with first-order perturbation theory. The above first-order perturbation formula is derived assuming the rotating wave approximation (RWA) (a good approximation since the energy difference between the XO_g^+ and $D1_u$ states is resonant with the bind pulse photon energy) and the Condon approximation where the electronic transition dipole moment is assumed to be independent of R, i.e., $\mu_{21}(R)\approx\mu_{21}$, a constant, taken here as 0.27 D.[40]

The only major difficulty in evaluating Eq. (10) is computing the Franck–Condon factors between the continuum states of $V_1(R)$ and the bound states of $V_2(R)$ which here are evaluated using semiclassical methods as outlined by Child:[41]

$$\begin{aligned}\langle\phi_2^{(m)}|\phi_E\rangle\propto&\sqrt{\frac{1}{\nu(R_x)}}\ \sqrt{\frac{1}{V_2'(R_x)-V_1'(R_x)}}\\&\times\sin\left[\int_{a_1(E)}^{R_x}dR'k_1(R')+\int_{R_x}^{a_2(E_m)}dR'k_2(R')\right],\end{aligned} \quad (11)$$

where $\nu(R_x)$ is the velocity at the crossing point R_x of the two potentials when they are shifted such that $E=E_m$, $a_1(E)$ is the classical turning point on $V_1(R)$ at energy E, $a_2(E_m)$ is the classical turning point on $V_2(R)$ at energy E_m, $k_1(R')=\sqrt{2m(E-V_1(R'))}/\hbar$, $k_2(R')=\sqrt{2m(E_m-V_2(R'))}/\hbar$, and $V_1'(R_x)$ and $V_2'(R_x)$ are the slopes of the potential curves at the crossing point.

Equation (10) provides the photoassociated population on $V_2(R)$ from a thermal distribution of continuum states of $V_1(R)$ via the bind pulse. Now we also require the population which is excited from $V_2(R)$ to the depletion state $V_3(R)$ via the subsequent probe pulse at different bind-probe time delays. If the wavefunction on $V_3(R)$ is expressed as a superposition of its bound eigenstates

$$|\psi_3(R,t)\rangle=\sum_n\ a_3^{(n)}(t)|\phi_3^{(n)}(R)\rangle, \quad (12)$$

then the total population on $V_3(R)$ is

$$\langle\psi_3(R,t)|\psi_3(R,t)\rangle=\sum_n\ |a_3^{(n)}(t)|^2. \quad (13)$$

For $t\gg t_{\rm probe}$, i.e., when the probe pulse is over, the eigenstate populations are, using second-order perturbation theory,

$$\begin{aligned}|a_3^{(n)}(t\gg t_{\rm probe})|^2=A_{\rm bind}^2A_{\rm probe}^2\frac{\mu_{32}^2\mu_{21}^2\pi^2}{16\hbar^2N^2\alpha^4}\Bigg[&\sum_E\ \sum_m\ |\langle\phi_3^{(n)}|\phi_2^{(m)}\rangle|^2|\langle\phi_2^{(m)}|\phi_E\rangle|^2S_1(n,m,E)\exp(-E/k_BT)\\&+2\sum_E\ \sum_{m'}\ \sum_{m''}^{m'-1}\ {\rm Re}\{\langle\phi_3^{(n)}|\phi_2^{(m')}\rangle\langle\phi_2^{(m')}|\phi_E\rangle S_2(n,m',E)S_2(n,m'',E)\langle\phi_3^{(n)}|\phi_2^{(m'')}\rangle\langle\phi_2^{(m'')}|\phi_E\rangle\}\Bigg].\end{aligned} \quad (14)$$

Here we have defined

$$S_1(n,m,E) = \exp[-(\omega_{nm}-\omega_{\text{probe}})^2/2\alpha^2] \times \exp[-(\omega_{mE}-\omega_{\text{bind}})^2/2\alpha^2], \quad (15a)$$

$$S_2(n,m,E) = \exp(i\omega_{nm}t_{\text{probe}})\exp(i\omega_{mE}t_{\text{bind}})d \times \exp[-(\omega_{nm}-\omega_{\text{probe}})^2/4\alpha^2] \times \exp[-(\omega_{mE}-\omega_{\text{bind}})^2/4\alpha^2]. \quad (15b)$$

Again, as in Eq. (10), the Franck–Condon factors between the continuum and bound states were evaluated semiclassically. The bound-bound Franck–Condon factors, $\langle \phi_3^{(n)} | \phi_2^{(m)} \rangle$, were evaluated numerically by first computing the bound eigenstates of $V_2(R)$ and $V_3(R)$ using the Fourier grid Hamiltonian (FGH) method.[42] It is worth noting that only the second term on the right hand side of Eq. (14) contains the relative timing of the bind and probe pulses; this is the ''interference'' term which gives rise to the variation of the $D1_u$ state population (and therefore the fluorescence) with respect to the bind-probe delay.

The above formulation, besides being similar to the previously mentioned works on time resolved photoassociation,[32–34] is also similar to that used by Krause *et al.* in their analysis of the femtosecond photodissociation transients of cyanogen iodide (ICN).[43] As in that work, we also employed time dependent perturbation theory to compute the radiative bind and probe transition probabilities and semiclassical approximations to evaluate the bound-continuum Franck–Condon factors. The major difference between the work of Krause *et al.*[43] and the ultrafast photoassociation works is that in these a thermal initial distribution of continuum states must be accounted for, whereas in the photodissociation work the initial state was a single bound eigenstate of the ICN potential well.

Before presenting results, some distinctions between the above formulation for modeling time resolved photoassociation and previous works should be made. First, the system in the work of Machholm *et al.*[33] was assumed to consist of ultracold (sub-mK range) sodium atoms, and so the range of significantly populated continuum states of the Na–Na ground electronic state was assumed to be very narrow. Thus, in that work, numerical integration over the Franck–Condon factors between the ground continuum and each vibrational state in the upper bound curve was unnecessary—the narrow range of populated continuum states justified setting all Franck–Condon factors to a constant. In our case, as in the other recent work on mercury,[34] a large thermal distribution of significantly populated continuum states must be assumed since the temperature is relatively large, and thus the Franck–Condon factors cannot be assumed to be a constant over the whole continuum range. In this work, these were evaluated semiclassically as described above; using the WKB method cuts down on the numerical effort involved in computing the Franck–Condon factors.

III. RESULTS

The simulated laser-induced fluorescence (LIF) signal from FPAS vibrational transients on the $D1_u$ state of mercury are shown in Fig. 2 as a function of bind-probe time delay. Results from both wave packet simulation (dashed line) and perturbative method (solid line) are shown. (For this figure a lower probe field intensity of 3.5×10^{12} W/cm^2 is assumed.) Generally, the structure and oscillatory pattern of the fluorescence signal from both methods is the same; the only major difference appears to be an overall scaling factor. Note the double humped structure in both cases—this is due to the fact that probing does not occur exactly at a turning point in the $D1_u$ state, therefore the wave packet which oscillates back and forth is probed twice per oscillation. This probing effect has been documented in previous femtosecond studies.[44]

The difference between the two methods might be due to the semiclassical evaluation of the continuum-bound Franck–Condon factors in the perturbative approach. Note the oscillation period of 0.3 ps. The bind-pulse energy is resonant with the energy difference between the XO_g^+ and $D1_u$ states at $R_{\text{res}}=2.82$ Å, i.e., $V_2(R_{\text{res}})-V_1(R_{\text{res}}) = \hbar\omega_{\text{pump}}$. The energy level corresponding to this position (i.e., the turning point) on $V_2(R)$ is $\nu=12$ for which the vibrational period is 0.29 ps, so the oscillation period we observe for the transient dynamics seems reasonable, particularly if the photoassociation process is viewed as a quasi-Franck–Condon transition.

The experimental data does not show the modulation depth and regularity of vibrational features that our theory predicts. One possible explanation for the difference in signal modulation depth on the vibrational time scale between theory and experiment could be that the present calculations are taking into account only one possible probe depletion state, the 1_g state. As discussed in Sec. I, there may be multiple states which are energetically nearby the 1_g state and are accessible to probing from the $D1_u$ state.

To assess this possibility, we performed perturbative calculations of the vibrational transients from the mercury FPAS experiment employing Morse potentials with identical parameters except for the equilibrium distance: 2.65, 3.15, and 3.65 Å. Figure 3 displays the average of these three signals. Note the apparent lack of a vibrational signature—the presence of other states near the 1_g state in Hg_2 is quite likely and may be responsible for the lack of ''sinusoidal'' vibrational signatures in the experimental data. A low amplitude irregular motion is more likely to be regarded as experimental noise. Analysis of the experimental transients in Ref. 16 once the rotational anisotropy has been removed reveals a high degree of correlation in their features. This correlation is not found in the same data for negative times or when one transient is displaced in time with respect to the other by a 40 or 80 fs step. While it is tempting to perform a more complete analysis and simulation of these data we remain cautious and are working on obtaining data with a higher signal-to-noise ratio.

In these calculations we have assumed that all Hg+Hg

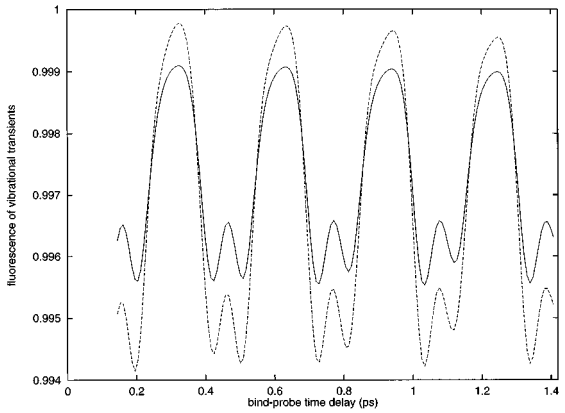

FIG. 2. Simulated FPAS signal as a function of bind-probe delay time showing the vibrational transients. Results form the wave packet propagation method (dashed line) and perturbative method (solid line) are shown. These transients show coherent oscillation dynamics in the photoassociated molecule even though they include an incoherent summation over the Boltzman distribution of continuum states at 433 K.

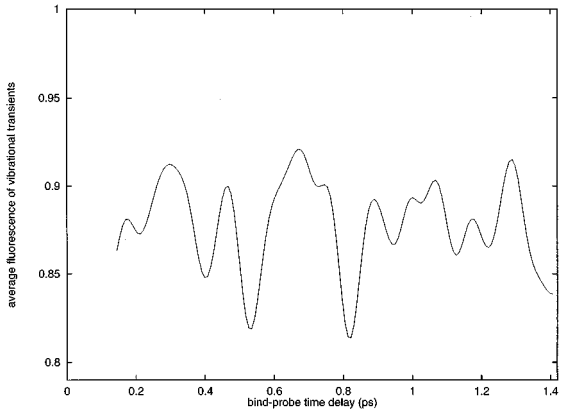

FIG. 3. Average of three perturbative calculations of vibrational transients using three 1_g potentials which differ only in the equilibrium bond distance; 2.65, 3.15, and 3.65 Å. Notice the decrease in modulation depth and the absence of a regular oscillation pattern as seen in Fig. 2.

collisional pairs which are photoassociated are zero impact parameter (head-on) collisions. Nonzero impact parameters translate into nonzero angular momenta of the mercury atom pairs and have the effect of raising all the interatomic potential curves by the same amount of centrifugal energy, $J(J+1)\hbar^2/(2mR^2)$. Thus the point of resonance, i.e., the point where $V_2(R)-V_1(R)=\hbar\omega_{\text{bind}}$, is independent of the impact parameter. However, the individual curve shapes do change due to the centrifugal term, thereby affecting the radiative transition probabilities. Given the large reduced mass of mercury, there is little distortion in the potential curves. Therefore, in terms of the computed vibrational transient signal, inclusion of nonzero impact parameter collisions in the computations, as done by Backhaus and Schmidt,[34] does not alter the results significantly (although it greatly increases the computational effort). The effects of collisions with impact parameters larger than zero on the angular momentum of the products, however, are significant *vide infra*.

IV. DISCUSSION AND IMPLICATIONS FOR CONTROL OF BIMOLECULAR REACTIONS

We have demonstrated here that it is possible (at least in principle) to observe coherent vibrational transients in bound←free FPAS experiments, even at high temperatures (>400 K). Both wave packet propagation and perturbative methods were used to compute the fluorescence from the FPAS vibrational transients. Both methods gave similar results, but the perturbative method requires nearly two orders of magnitude less computational time, and it therefore may be a more promising method for simulating FPAS experiments in multidimensional systems.

While the decay of rotational anisotropy in the FPAS experiment[16] clearly indicated that femtosecond photoassociation had occurred, vibrational transients were not conclusively observed. As demonstrated in the previous section, other probe depletion states may be responsible for the irregular and low amplitude vibrational signal. An alternative detection method which provides a background-free signal from a single upper electronic state might be helpful in this regard and is currently being considered.

Finally, as mentioned in Sec. I, the FPAS method may be used as a tool in the control of bimolecular reactions. Ultrafast laser control of bimolecular was first considered by Krause *et al.*[27] In that work, the reactions of $H+H_2$ and $D+H_2$ were controlled by a two pulse experiment. Their calculations considered collinear collisions (zero impact parameter) with a very narrow range of translational energies (a monoenergetic molecular beam would be required).

Using the FPAS method we show that orientation and impact parameters may in general be controlled to some extent in bimolecular reactions. Specifically, alignment is controlled in FPAS by the polarization of the binding laser since only collision pairs with a transition dipole oriented along the electric field vector of the laser are photoassociated. FPAS also allows for some degree of control over the collision energy by selecting out and photoassociating only those pairs of atoms which are within a certain energy range. To see this, consider a head-on collision between two mercury atoms. As mentioned in the previous section, a radiative transition will most likely occur at $R_{\text{res}}=2.82$ Å. Roughly speaking, for collisions energies E_{rel} less than $V_1(R_{\text{res}}) = 0.093$ eV, the diatom pairs cannot photoassociate because they do not possess sufficient translational energy to reach the resonance point. Thus low energy collision pairs are excluded from the photoassociation process.

As for the control of the impact parameter of the photoassociating pairs of atoms, we first note that when considering nonzero impact parameters ($J>0$), the relative collision energy for photoassociation must satisfy the condition

$$E_{\text{rel}} > V_1(R_{\text{res}}) + \frac{J(J+1)\hbar^2}{2m(R_{\text{res}})^2} \tag{16}$$

in order for photoassociation to occur. Therefore, collisions with large impact parameters (corresponding large J) are

also excluded from photoassociation since large impact parameter collisions will have to possess very high collisional energies.

With a tunable binding laser it is possible to control the impact parameter by varying the binding laser wavelength, λ_{bind}. The degree of control that one may exert over the impact parameter of the collision atom pairs which are photoassociated can be demonstrated as follows. First, we assume that the binding laser is resonant with the energy difference between the $D1_u$ and XO_g^+ states at some distance $R'=R_{\text{res}}$, i.e., $V_2(R')-V_1(R')=\hbar\omega_{\text{bind}}$. Second, the slope $V_2(R')-V_1(R')/\Delta R$ near R' is large compared to the bandwidth of the excitation pulse such that even for femtosecond pulses the excitation may be considered to be localized. In our specific case, the slope $V_2(R')-V_1(R')/\Delta R$ calculated at R' is $\approx 11\,000\ \text{cm}^{-1}/\text{Å}$ and the bandwidth is $\approx 350\ \text{cm}^{-1}$ for our 42 fs bind pulse width. Third, the major contribution to the Franck–Condon overlap between the ground state continua and the excited bound state come from a narrow region about R', the resonance distance. Therefore only those pairs of atoms near R' are photoexcited (a strict resonance condition).

Armed with these assumptions, we see that for a given collision energy E, the impact parameter b must satisfy the condition

$$b \leqslant R' \sqrt{\frac{E-V_1(R')}{E}} \tag{17}$$

in order for photoassociation to take place. Conversely, for a collision pair with a given impact parameter b, the collision energy must satisfy the condition

$$E \geqslant \frac{V_1(R')}{1-(b/R')^2}. \tag{18}$$

Assuming the above conditions for a ''successful'' collision, i.e., one in which the two atoms can come within a distance of R' or less, we may derive an expression for the total photoassociation cross-section:

$$\sigma_{\text{total}} = N \int_{V_1(R')}^{\infty} dE\ \exp(-E/k_BT) \times \int_0^{R'} \sqrt{\frac{E-V_1(R')}{E}}\, db(2\pi b), \tag{19}$$

where N is the normalization constant $1/(k_BT)$ or, reversing the order of integration,

$$\sigma_{\text{total}} = N \int_0^{R'} db(2\pi b) \int_{\frac{V_1(R')}{1-(b/R')^2}}^{\infty} dE\ \exp(-E/k_BT) = \int_0^{R'} db(2\pi b) \exp\left(-\frac{V_1(R')}{[1-(b/R')^2]k_BT}\right). \tag{20}$$

Note that the upper limit in the integral in Eq. (20) is R'; collisions between atoms with impact parameters greater than R' obviously cannot approach distances shorter than R', therefore, they cannot be photoassociated. However, if the upper limit of this integral is set at some other value, say b', where $0<b'<R'$, then we have defined a ''restricted'' cross-section which accounts for collision impact parameters from zero to b' only:

$$\sigma_{\text{restricted}} = \int_0^{b'} db(2\pi b) \exp\left(-\frac{V_1(R')}{[1-(b/R')^2]k_BT}\right). \tag{21}$$

The quantity $\sigma_{\text{restricted}}/\sigma_{\text{total}}$ is therefore the fraction of photoassociated molecules which are created from collision pairs with impact parameters in the limited range below b'.

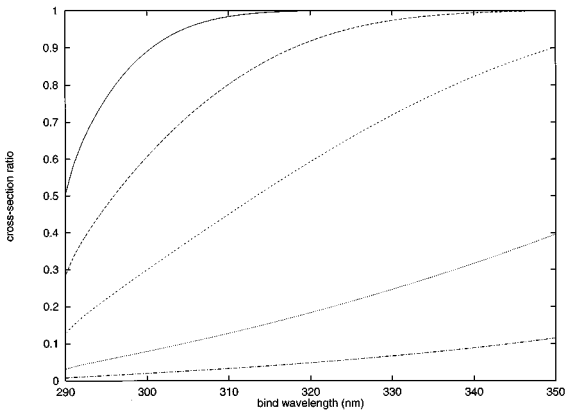

FIG. 4. Variation of cross-section ratio $\sigma_{\text{restricted}}/\sigma_{\text{total}}$ as a function of binding wavelength λ_{bind} for five impact parameter ranges (in order lower to upper curves): 0.26, 0.53, 1.06, 1.59, and 2.12 Å (see text).

Since $\sigma_{\text{restricted}}/\sigma_{\text{total}}$ depends on R', and since λ_{bind} defines R' due to the requisite resonance condition, this ratio may be controlled by varying the bind laser wavelength. In Fig. 4 the cross-section ratio versus λ_{bind} is plotted for restricted impact parameter (b') values of 0.26, 0.53, 1.06, 1.59, and 2.12 Å. The range of binding wavelengths varies from 290 to 370 nm which samples the region from $R'=2.53$ to 3.07 Å; this entire range is in the continuum region of the ground state potential, i.e., $V_1(R')>0$. As expected, the larger the restricted impact range (2.12 Å curve), the larger the cross-section ratio. However, note the significant amount of control over the impact parameter of photoassociated collision pairs shown in Fig. 4. In particular, the ratio corresponding to the restricted impact parameter range $0<b<1.06$ Å changes by nearly an order of magnitude over the range of binding wavelengths shown. Thus at ($\lambda_{\text{bind}}=350$ nm) 90% of the photoassociated molecules have impact parameters in the restricted range $0<b<1.06$ Å, and at the other extreme ($\lambda_{\text{bind}}=290$ nm) almost 90% of the photoassociated molecules are created from collision pairs with impact parameters greater than 1.06 Å.

Another way to graphically visualize the control over impact parameter with bind laser wavelength is shown in Fig. 5. Here the normalized impact parameter distribution

$$P(b) = \left(\frac{1}{\sigma_{\text{total}}}\right) 2\pi b\ \exp\left\{-\frac{V_1(R')}{[1-(b/R')^2]k_BT}\right\} \tag{22}$$

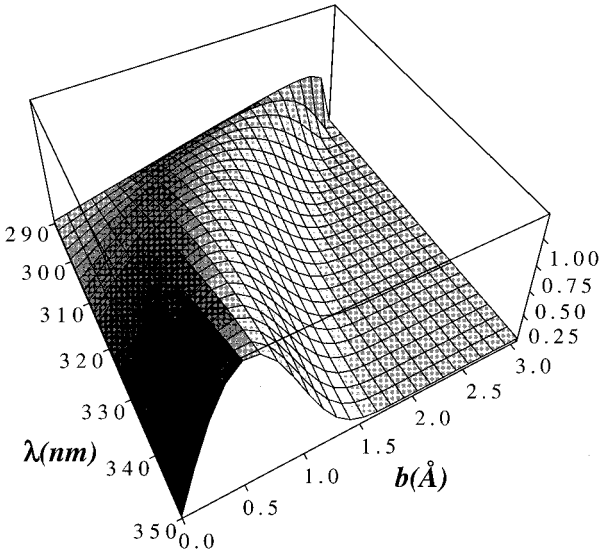

FIG. 5. Plot of impact parameter distributions for a range of binding wavelengths (290–350 nm). Long wavelengths yield small impact parameters $b < 1$ Å while short wavelengths yield large impact parameters $b > 2$ Å.

is plotted for bind wavelengths ranging from $\lambda_{\text{bind}}=290$ to 350 nm [the normalization, i.e., the total cross-section σ_{total} is given in Eq. (20)]. Note that both the peak and width of the impact parameter distribution change significantly as a function of λ_{bind}.

Controlling the impact parameter as described above opens up the possibility of controlling the angular momentum of the photoassociated products. If, as in a molecular beam apparatus, one was able to restrict the collision energies to a narrow monoenergetic range, then controlling the impact parameter b would also allow for control of the angular momentum since classically the angular momentum is equivalent to $m\nu b$ where $\nu=\sqrt{2E/m}$. Furthermore, as shown in Fig. 5, a narrow range of velocities would allow for control over the angular momentum distribution as well.

Finally, in terms of controlling bimolecular reactions, FPAS provides a time zero for chemical bond formation between a thermal gas of unbound atoms or molecules. Because of the short duration of the pulse, only those collision pairs near a specific internuclear distance (R_{res}) will be photoassociated. Thus energy, impact parameter, and orientation can be controlled to some extent in bimolecular reactions occurring in thermal samples of free reactants. Application of FPAS to more complicated systems involving collisions between molecules are underway in our laboratory.

ACKNOWLEDGMENTS

We thank Dr. Pao-Hua Liu for her contributions in the preliminary part of this work. M.D. would like to thank Professor J. Manz and Professor R. Kosloff for insightful discussions about ultrafast photoassociation, and P. Backhaus and B. Schmidt for providing us with a preprint of their work. P.G. and M.D. would also like to thank Professor R. Cukier for valuable discussions about the statistical mechanics of these processes. Partial support from a Camille and Henry Dreyfus New Faculty Award is acknowledged. M.D. is a Beckman Young Investigator, and a Packard Science and Engineering Fellow.

[1] S. Mrozowski, Z. Physik **106**, 458 (1937).
[2] R. O. Doyle, J. Quant. Rad. Spec. Transfer **8**, 1555 (1968).
[3] V. S. Dubov, L. I. Gudzenko, L. V. Gurvich, and S. I. Iakovlenko, Chem. Phys. Lett. **45**, 330 (1977).
[4] D. B. Lidov, R. W. Fakone, T. F. Young, and S. E. Harris, Phys. Rev. Lett. **36**, 462 (1976).
[5] G. Inoue, J. K. Ku, and D. W. Setser, J. Chem. Phys. **80**, 6006 (1984).
[6] J. D. Miller, R. A. Cline, and D. J. Heinzen, Phys. Rev. Lett. **71**, 2204 (1993).
[7] R. Napolitano, J. Weiner, C. J. Williams, and P. S. Julienne, Phys. Rev. Lett. **73**, 1352 (1994).
[8] P. D. Lett, P. S. Julienne, and W. D. Philips, Annu. Rev. Phys. Chem. **46**, 423 (1995).
[9] H. R. Thorsheim, J. Weiner, and P. S. Julienne, Phys. Rev. Lett. **58**, 2420 (1987).
[10] R. B. Jones, J. H. Schloss, and J. G. Eden, J. Chem. Phys. **98**, 4317 (1993).
[11] J. H. Schloss, R. B. Jones, and J. G. Eden, Chem. Phys. Lett. **191**, 195 (1992).
[12] E. B. Gordon, V. G. Egorov, S. E. Nalivaiko, V. S. Pavlenko, and O. S. Rzhevsky, Chem. Phys. Lett. **242**, 75 (1995).
[13] R. A. Cline, J. D. Miller, and D. J. Heinzen, Phys. Rev. Lett. **73**, 632 (1994).
[14] T. Bergeman and P. Liao, J. Chem. Phys. **72**, 886 (1980).
[15] H. Scheingraber and C. R. Vidal, J. Chem. Phys. **66**, 3694 (1977).
[16] U. Marvet and M. Dantus, Chem. Phys. Lett. **245**, 393 (1995).
[17] M. C. Castex, J. Chem. Phys. **66**, 3854 (1977).
[18] J. L. Carlsten, A. Szoke, and M. G. Raymer, Phys. Rev. A **15**, 1029 (1977).
[19] B. R. Johnson, C. Kittrell, P. B. Kelley, and J. L. Kinsey, J. Phys. Chem. **100**, 7743 (1996).
[20] M. J. Rosker, M. Dantus, A. H. Zewail, J. Chem. Phys. **89**, 6113 (1988); M. Dantus, M. J. Rosker, and A. H. Zewail, *ibid.* **89**, 6128 (1988).
[21] J. Misewich, J. H. Glownia, J. E. Rothenberg, and P. P. Sorokin, Chem. Phys. Lett. **150**, 374 (1988).
[22] J. H. Glownia, J. A. Misewich, and P. P. Sorokin, J. Chem. Phys. **92**, 3335 (1990).
[23] N. F. Scherer, L. R. Khundkar, R. B. Bernstein, and A. H. Zewail, J. Chem. Phys. **87**, 1451 (1987).
[24] J. P. Visticot, B. Soep, and C. J. Whitham, J. Phys. Chem. **92**, 4574 (1988).
[25] S. I. Ionov, G. A. Brucker, C. Jaques, L. Valachovic, and C. Wittig, J. Chem. Phys. **99**, 6553 (1993).
[26] E. D. Potter, J. L. Herek, S. Pedersen, Q. Lin, and A. H. Zewail, Nature **355**, 66 (1992).
[27] J. L. Krause, M. Shapiro, and P. Brumer, J. Chem. Phys. **92**, 1126 (1990).
[28] T. Mercouris, I. D. Petsalakis, and C. A. Nicolaides, Chem. Phys. Lett. **208**, 197 (1993).
[29] I. D. Petsalakis, T. Mercouris, and C. A. Nicolaides, Chem. Phys. **189**, 615 (1994).
[30] F. H. Mies and A. L. Smith, J. Chem. Phys. **45**, 994 (1966).
[31] F. H. Mies, J. Chem. Phys. **48**, 482 (1967).
[32] J. Jiang and J. S. Hutchinson, J. Chem. Phys. **87**, 6973 (1987).
[33] M. Machholm, A. Giusti-Suzor, and F. H. Mies, Phys. Rev. A **50**, 5025 (1994).
[34] P. Backhaus, J. Manz, and B. Schmidt, Adv. Chem. Phys. (to be published); P. Backhaus and B. Schmidt, Chem. Phys. (in press).
[35] M. Dantus, R. M. Bowman, and A. H. Zewail, Nature **343**, 737 (1990); A. H. Zewail, J. Phys. Chem. **97**, 12 427 (1993).
[36] *Femtosecond Chemistry*, edited by J. Manz and L. Woste (VCH, Weinheim, 1995).
[37] V. Engel and H. Metiu, J. Chem. Phys. **90**, 6116 (1989).
[38] V. Engel and H. Metiu, J. Chem. Phys. **91**, 1596 (1989).
[39] R. Kosloff, J. Phys. Chem. **92**, 2087 (1988).

[40] R. J. Hay, T. H. Dunning, and R. C. Raffenetti, J. Chem. Phys. **65**, 2679 (1976).
[41] M. S. Child, *Semiclassical Mechanics with Molecular Applications* (Oxford University Press, New York, 1991).
[42] C. C. Marston and G. G. Balint-Kurti, J. Chem. Phys. **91**, 3571 (1989).
[43] J. L. Krause, M. Shapiro, and R. Bersohn, J. Chem. Phys. **94**, 5499 (1991).
[44] A. Mokhtari, P. Cong, J. L. Herek, and A. H. Zewail, Nature **348**, 225 (1990).
[45] J. Koperski, J. B. Atkinson, and L. Krause, Can. J. Phys. **72**, 1070 (1994).
[46] R. J. Niefer, J. Supronowicz, J. B. Atkinson, and L. Krause, Phys. Rev. A **35**, 4629 (1987).